# Investigation of urban heat island and carbon monoxide change using Google Earth engine in Konya

## Konya'da kentsel ısı adası ve karbon monoksit değişiminin Google Earth engine kullanılarak incelenmesi

**Duygu Arıkan[1,*]** iD **, Ferruh Yıldız[2]** iD

[1,2] *Konya Technical University, Department of Geomatics Engineering, 42250, Konya, Türkiye*

**Abstract**

The increasing population has been causing changes in and around urban areas. As a result of this situation, it is observed that the amount of heat and air pollution in cities is higher than in rural areas. Urban heat islands (UHI) are a factor that affects people's quality of life. Therefore, monitoring temperature changes and taking regional measures is necessary. In this study, urban heat island (UHI) and carbon monoxide (CO) levels were determined using Landsat 8 satellite for the years 2019-2021 and Sentinel-5P satellite, respectively. The central districts of Konya were selected as the study area. To determine the urban heat island (UHI), surface temperature (ST) maps were created using the thermal band of a total of 12 Landsat 8 satellite images for each season. Additionally, 36 CO maps were generated using the Sentinel-5P satellite for the same region, covering twelve months. Upon evaluation of the generated maps, a significant correlation between temperatures and CO was observed. It was determined that areas with higher surface temperature also exhibited higher levels of carbon monoxide.

**Keywords:** Urban heat islands, Land surface temperature, Air quality, Carbon monoxide, National air quality monitoring station

**Öz**

Nüfusun artması kentlerde ve çevresinde değişiklikler meydana getirmektedir. Bu duruma bağlı olarak kentlerdeki ısı miktarı ve hava kirliliğinin kırsal alana göre daha fazla olduğu gözlemlenmektedir. Kentsel ısı adası insanın yaşam kalitesini etkileyen bir faktördür. Bu sebeple ısı değişikliklerinin izlenmesi, bölgesel olarak tedbir ve önlemlerin alınması gerekmektedir. Bu çalışmada, 2019 – 2021 yılları arasında Landsat 8 uydusu kullanılarak kentsel ısı adası ve Sentinel-5P uydusu kullanılarak karbonmonoksit (CO) durumu belirlenmiştir. Çalışma bölgesi olarak Konya'nın merkez ilçeleri seçilmiştir. Kentsel ısı adasını (KIA) belirlemek için her mevsime ait toplam 12 adet Landsat 8 uydu görüntüsünün termal bandı kullanılarak yer yüzey sıcaklığı (YYS) haritaları oluşturulmuştur. Ayrıca aynı bölge için Sentinel-5P uydusu kullanılarak on iki aya ait 36 adet CO haritası oluşturulmuştur. Oluşturulan haritalar değerlendirildiğinde sıcaklık ve CO arasında anlamlı bir sonuç olduğu belirlenmiştir. YYS sıcaklığının fazla olduğu kısımlarda karbonmonoksit miktarının fazla olduğu tespit edilmiştir.

**Anahtar kelimeler:** Kentsel ısı adası, Yer yüzey sıcaklığı, Hava kalitesi, Karbon monoksit, Ulusal hava kalitesi izleme istasyonu

## 1 Introduction

The increase in air temperatures in urban areas compared to rural areas due to climate change is referred to as the "heat island" phenomenon [1]. The differentiation that occurs as a result of human factor and climate effects has emerged as the concept of "urban heat island" [1-4].

The occurrence of climate change depends on both external factors and naturally occurring internal factors. For example, human-induced changes in land use can be one factor, while changes in the composition of the atmosphere can be another factor [5]. Many studies have proven that changes in the land surface and land uses have an impact on the urban heat island [6-8].

According to the United Nations population data, the majority of the world's population lives in urban areas and their numbers are increasing. As of 2021, Turkey constitutes 1.1% of the world population with 84 million 680 thousand 273 people [9]. The increasing human population leads to

efforts to meet the needs of urban areas, resulting in an increase in building construction, electricity consumption, transportation time, and use of fuels for heating purposes. These factors increase gas emissions into the atmosphere. The excessive rise in temperature can affect the quality of life for urban residents, leading to health problems [10,11] To ensure human life can continue in a region, it is important to consider anthropogenic emissions, heat sources, vegetation coverage and soil impermeability, as they are crucial for human health and life [3,12,13]. Therefore, to ensure environmental sustainability, climate-friendly approaches such as preserving natural resources, reducing waste, increasing energy efficiency, implementing sustainable transportation systems, and increasing green areas should be adopted in urban areas.

Remote sensing data has enabled monitoring of both spatial and temporal changes on Earth, as well as offering solutions [14]. Advances in satellite technology have

NÖHÜ Müh. Bilim. Derg. / NOHU J. Eng. Sci. 2023; 12(4), 1185-1193

D. Arıkan, F. Yıldız

impacted sensor platforms and acquired various types of data (such as optical, thermal, and emission) easier [8,14-17]. Landsat, Aster, and Modis satellites offer free access to both thermal and optical data. Also, another example is the Sentinel satellite mission, which launched Sentinel-1 and Sentinel-2 satellites in 2015 to provide radar and optical data, and Sentinel-5P in 2017 to determine gas density in the atmosphere. The Sentinel-3 satellite, which has a thermal band, is aimed at environmental and climate monitoring [18].

In parallel with this development in satellite technology, new tools have been developed to analyze, evaluate, and model data [19]. One of these tools is the Google Earth Engine (GEE) software. It is a web-based software launched by Google in 2010 [19]. In addition to providing free access to users, it contains a data catalog that covers approximately 40 years of data. As a result, it is widely used to quickly analyze and interpret data in monitoring environmental changes (such as land cover/land use, disasters, climate change, soil, wetland or drought, forest and urban areas) [20-24].

There are weather stations that measure the temperature in urban and rural areas. However, various studies have shown that these stations are not evenly distributed over their working areas or do not allow for the global determination of temperature [25]. Therefore, in our study, UHI was calculated based on the three central districts of Konya, namely Karatay, Meram and Selçuklu, between 2019-2021,

and the UHI situation was examined using satellite imagery. In addition, carbon monoxide levels in the same region and time period were examined and their relationship was evaluated. Carbon monoxide data obtained from air quality stations in the region were also taken into account in the results.

## 2 Material and method

### 2.1 Study area

Konya, chosen as the study area, is the city with the largest surface area (39.000 km²) in Turkey. It is located between 36° 22' and 39° 08' north parallels and 31° 14' and 34° 05' east meridians (Figure 1). The city, which is one of the developed cities of the country, has a total of thirty-one districts. The current population announced by TUIK in 2021 is 2,277,017, making it the sixth most populous province in the country [9]. The most populous district of the city is Selçuklu. The city, which has a hot and dry climate in summer and a cold and snowy climate in winter, has a terrestrial climate in general [26].

### 2.2 Data used

The UHI and carbon monoxide data were obtained from the Google Earth Engine (GEE) platform, which provides open access.
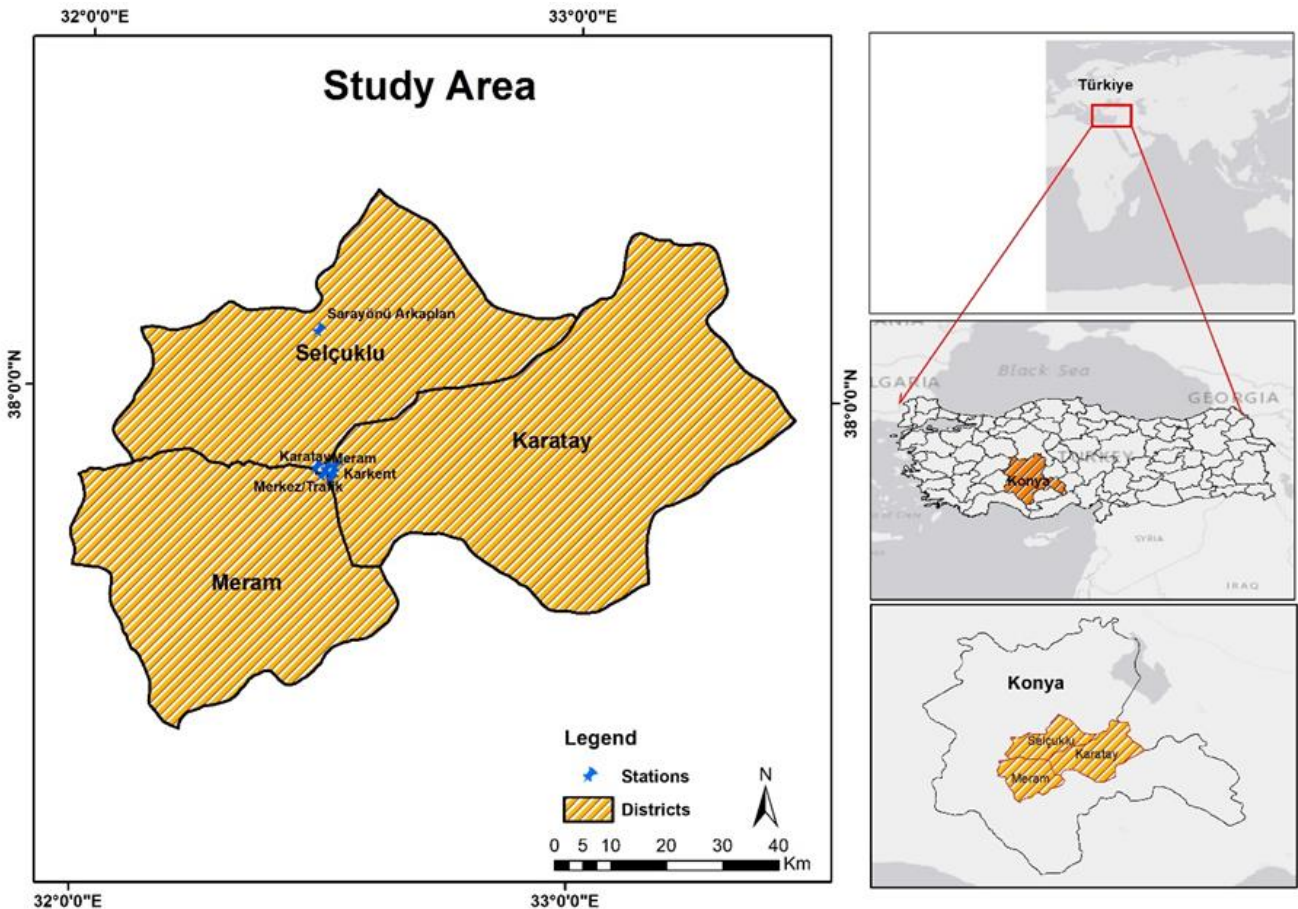


**Figure 1.** Study area (Three central districts of Konya city)

As a web-based application, it can run operations independently of the computer [27]. The application, developed in Python and JavaScript programming languages, consists of four parts in its interface (Figure 2). The first part contains the working files and a library consisting of sample codes within the program. The second part is an area where codes are written in the appropriate format and queries are made [28]. The third part provides the production of data results and allows them to be export, and the fourth part runs the visualization processes of the results. Data processing is done quickly and easily, and the results can be visualized. Additionally, as it runs in the cloud, it provides access to many satellite data over a wide date range within the platform [29]. In this study, Landsat-8 satellite imagery was used for the urban heat island, and Sentinel-5 satellite images were used for the carbon monoxide data.

Landsat 8 OLI/TIRS satellite was launched in 2013. The OLI sensor of the satellite consists of a 15-meter panchromatic band and eight multispectral bands with a 30-meter resolution. The satellite has a total of 11 bands, where the 10th and 11th bands are thermal bands [30]. The data can be accessed for free from the United States Geological Survey (USGS) [31]. The thermal bands of the satellite are mostly used in UHI studies [32-34].

In this study, the first thermal band of the satellite, the 10th band with has a 16-bit radiometric resolution, was preferred [30]. Because Yu, Guo, & Wu [35] and Jin, et. al, [36] used both thermal bands of the Landsat 8 satellite in their study. In line with the findings they obtained, it was determined that the 11th band value used to determine UHI was largely inconsistent with the other thermal band value [37, 38]. The wavelength of the thermal band used is 10.60 - 11.19 μm [30].

The Sentinel satellite mission has been providing radar and optical data since 2015 [39]. It also contributes to the determination of gaseous pollutants in the atmosphere thanks to the Sentinel-5 satellite images sent by the European Space Agency on October 13, 2017 [39]. There is information on 14 different air pollutants such as carbon monoxide (CO), nitrogen dioxide ($NO_2$), methane ($CH_4$), formaldehyde (HCHO), aerosol (AER_AI), sulfur dioxide ($SO_2$) and ozone($O_3$).

With the help of various satellite images, detecting and analyzing LST is carried out cost-effectively and quickly. The spectral brightness data of the Landsat-8 satellite can be converted to the supra-atmospheric luminosity temperature using the constant thermal values (Table 1) found in the satellite data file. Afterward, LST can be calculated (Figure 3).

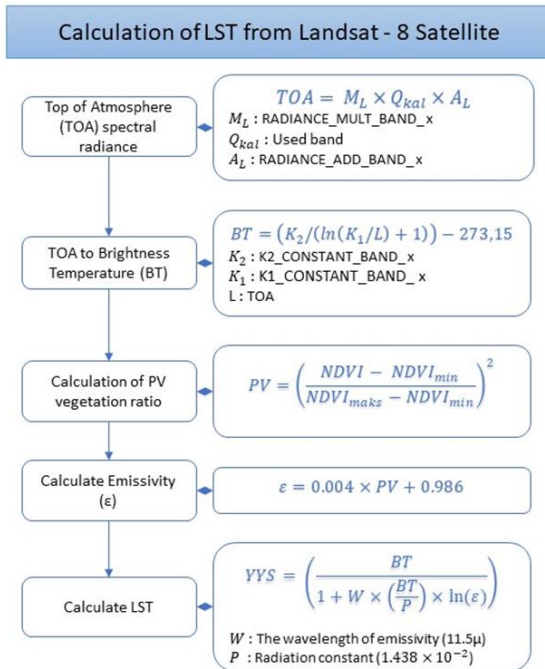**Table 1.** Thermal constant values of Landsat-8 satellite

| | |
|---|---|
| Radiance_Add_Band_10 | 0.10000000149011612 |
| Radiance_Mult_Band_10 | 0.00033420001273043454 |
| K1_Constant_Band_10 | 774.8853149414062 |
| K2_Constant_Band_10 | 1321.078857421875 |

To determine the LST (Land Surface Temperature), it is necessary to first calculate the spectral brightness values of the thermal band's values to be used, and then convert them [40]. In this study, the 10th band of the satellite was used as the thermal band. Then, using the spectral reflection value, the brightness values are converted into temperature values. For this, the calibrated K1 and K2 coefficients are used before the satellite is sent [40, 41]. The coefficient K1 is used to determine the relationship between measured radiation values. By multiplying the measured radiation values of a pixel with $K_1$, the pixel's surface temperature is converted.
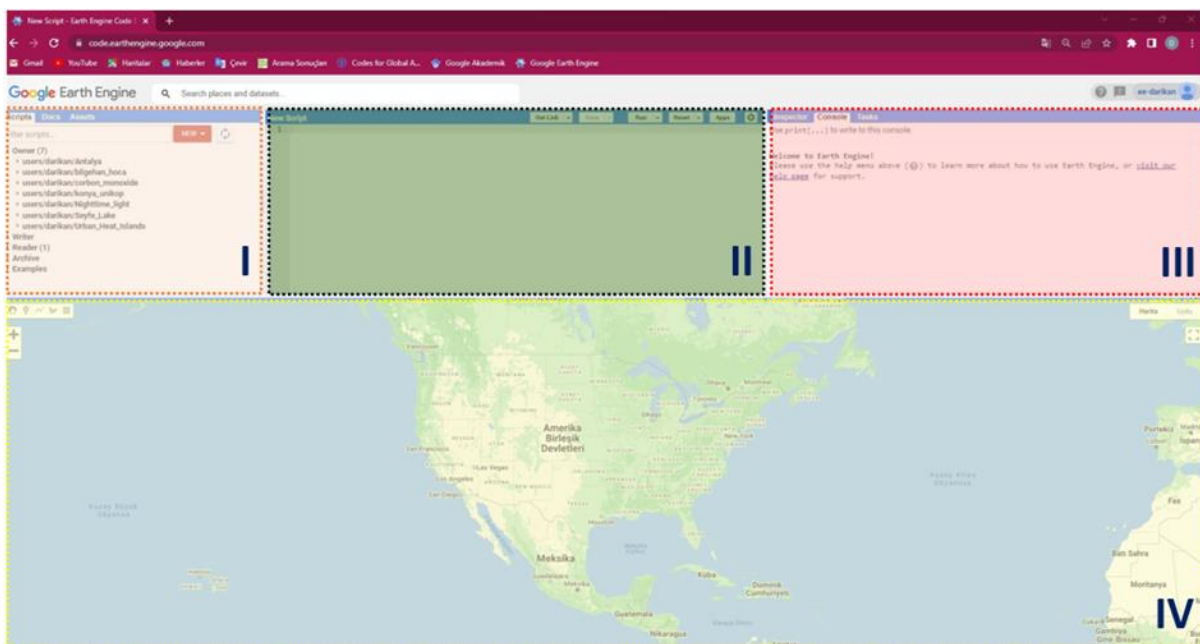


**Figure 2.** The interface of GEE software

The coefficient $K_2$, on the other hand, is used to determine the relationship between radiation values with higher sensitivity. After multiplying the pixel's radiation value with the $K_1$ coefficient, the $K_2$ coefficient is added, resulting in the pixel's surface temperature.



**Calculation of LST from Landsat - 8 Satellite**

**Top of Atmosphere (TOA) spectral radiance**
$$TOA = M_L \times Q_{kal} \times A_L$$
$M_L$ : RADIANCE_MULT_BAND_x
$Q_{kal}$ : Used band
$A_L$ : RADIANCE_ADD_BAND_x

**TOA to Brightness Temperature (BT)**
$$BT = \left(K_2/(ln(K_1/L) + 1)\right) - 273,15$$
$K_2$ : K2_CONSTANT_BAND_x
$K_1$ : K1_CONSTANT_BAND_x
L : TOA

**Calculation of PV vegetation ratio**
$$PV = \left(\frac{NDVI - NDVI_{min}}{NDVI_{maks} - NDVI_{min}}\right)^2$$

**Calculate Emissivity (ε)**
$$\varepsilon = 0.004 \times PV + 0.986$$

**Calculate LST**
$$YYS = \left(\frac{BT}{1 + W \times \left(\frac{BT}{P}\right) \times \ln(\varepsilon)}\right)$$
$W$ : The wavelength of emissivity (11.5µ)
$P$ : Radiation constant (1.438 × 10$^{-2}$)

**Figure 3.** Process steps to calculate LST

In summary, the $K_1$ and $K_2$ coefficients are used to calculate the land surface temperature using thermal infrared data. These coefficients can vary depending on the characteristics of remote sensing systems and the sensors used. The reason for subtracting the value 273.15 in the conversion to Brightness Temperature (BT) is to adjust the result obtained in kelvins in degrees Celsius. As a result, a temperature value has been calculated, but emissivity correction must be made in order to determine the LST. In order to calculate the emissivity value (ε), it is necessary to know the PV vegetation ratio. For this, the NDVI (Normalized Difference Vegetation Index) vegetation index is used. This index gives information about the health status or growth of the plant as a result of measuring the bright intensities of different wavelengths reflected by the plants on the ground [42]. The NDVI vegetation index is calculated using the near infrared and red bands found in satellites. The main reason for using these bands is that the wavelengths at which plants are most efficient for photosynthesis are determined as red and infrared light [43,44]. The mathematical model of the NDVI index is given in Equation 1.

$$NDVI = \frac{NIR - RED}{NIR + RED} \tag{1}$$

Using the equation, $NDVI_{min}$ and $NDVI_{max}$ values are calculated. Thanks to the data given in Table 1, the process

steps and mathematical expressions for the calculation of LST are briefly summarized in Figure 3.

## 3 Findings and discussion

Changes in cities are the areas most affected by climate change, although they cause climate change. In short, climate change and its impact in cities are directly proportional. For this reason, climate change and urban planning have become two concepts that cannot be considered separately from each other.

Landsat 8 satellite images were used to create the LST maps for 2019, 2020, and 2021, and the LST maps were created in the QGIS environment. Urban heat islands for 2019–2021 were examined as four seasons (spring, summer, autumn, and winter). Since there is a lack of data for the winter season of 2019, those parts are shown in white on the map. When examined at the winter season maps of 2020 and 2021, the average urban heat island is 6 degrees Celsius, while the amount of heat is lower in 2019. The temperature increases in the transition from winter to spring. Considering the effect of this situation, it was observed that the amount of urban heat increased in the spring season (Figure 4). In 2020, the heat was evenly distributed over the surface, around 21.30 ºC on average. The amount of heat in 2021 has increased in some parts compared to other years, and it is reflected on the map, especially in the city center and parts of the transportation lines.

The annual heat amount of the maps created in Figure 4, depending on the seasons, is also expressed in Figure 5. In the spring season, the temperature of 2021 increased by 2.36 ºC compared to 2019 and by 5.57 ºC compared to 2020. While the ground surface temperature is around 34 °C in 2019 and 2020 in summer, it is 36.83 °C in 2021. While there is a decrease in ground surface temperature in the transition from summer to autumn in 2020 and 2021, it is seen that there is not much change in temperature in 2019.

In the study, it was discussed whether the heat situation in the urban area has a relationship with one of the air pollutants, carbon monoxide. For this purpose, both terrestrial data and remote sensing technology were used. Air quality monitoring stations installed in our country were used for terrestrial data. These stations were established by the Turkish Ministry of Environment, Urbanization and Climate Change to be homogeneous throughout the country. When they were first installed in Erzurum and Samsun in 2015 to monitor air quality, they only collected sulfur dioxide ($SO_2$) and particulate matter data. Today, nitrogen dioxide ($NO_2$), ozone ($O_3$) data and carbon monoxide (CO) data used in the study are also collected and are freely accessible [45]. The number of stations has been increasing day by day since the year it was established and as of 2022, there are 360 air quality stations. The number of stations in Konya is 12. While the number of stations established in Karatay, Selçuklu and Meram districts was 4 in 2019, it doubled in 2021. The carbon monoxide data collected by the stations in the study region and time interval are presented in Table 2.
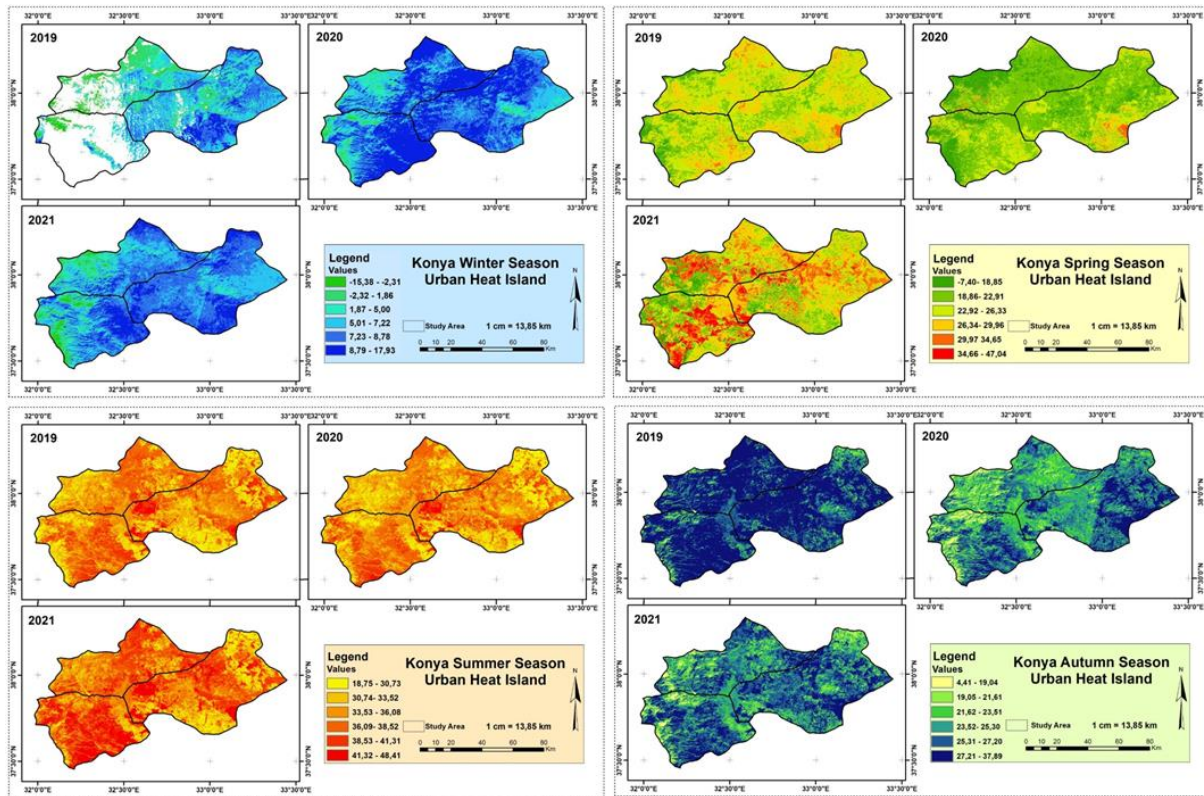
**Figure 4.** Urban heat islands in 2019-2021

**Table 2.** Carbon monoxide data obtained from the national air quality monitoring station

| Year | Station Name | Minimum Value(mg/m³) | Maximum Value(mg/m³) | Mean Value(mg/m³) | Number of Data (day) |
|------|-------------|-----------|-----------|-----------|----------|
| 2019 | Karkent | 306.68 | 3795.02 | 743.58 | 202 |
|      | Meram | 763.42 | 9090.62 | 1361.51 | 203 |
|      | Erenköy-Belediye | 92.75 | 3204.99 | 527.76 | 363 |
|      | Karatay | 95.38 | 5263.03 | 802.15 | 327 |
| 2020 | Karkent | 192.25 | 2362.75 | 613.06 | 362 |
|      | Meram | 17.86 | 4115.3 | 914.49 | 363 |
|      | Laboratuvar Yaygınlaştırma | 71.93 | 1662.19 | 376.42 | 136 |
|      | Erenköy-Belediye | 76.51 | 1754.42 | 514.87 | 354 |
|      | Karatay | 60.55 | 4939.74 | 662.98 | 341 |
|      | Karatay (SunayPark) | 88.53 | 5847.2 | 911.49 | 237 |
| 2021 | Karkent | 175.45 | 3948.49 | 663.56 | 323 |
|      | Meram | 205.8 | 8357.07 | 903.29 | 335 |
|      | Merkez/Trafik | 68.69 | 5892.96 | 828.82 | 243 |
|      | Laboratuvar Yaygınlaştırma | 87.67 | 3539.13 | 429.28 | 197 |
|      | Erenköy-Belediye | 151.13 | 3072.53 | 503.07 | 289 |
|      | Karatay | 38.57 | 12161.5 | 1774.87 | 79 |
|      | Sarayönü Arkaplan | 82.31 | 667.59 | 219.55 | 238 |
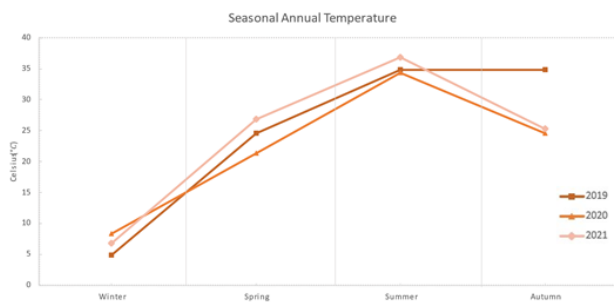


**Figure 5.** Annual urban heat island situation depending on the seasons (2019-2021)

Due to the lack of data at some stations and for better spatial analysis, Sentinel-5P satellite images was used for carbon monoxide data. GEE was used to obtain carbon monoxide maps. Visualization of result products made use of QGIS. The relationship between the change in air quality and temperature during the 36-month period (2019 January - 2021 December) in the central districts of Konya is discussed (Figure 6).

When the annual carbon monoxide maps are examined, it is seen that the rate in the winter season is higher than in the summer season. One of the main reasons for this is the increase in fuel used for heating in the winter.
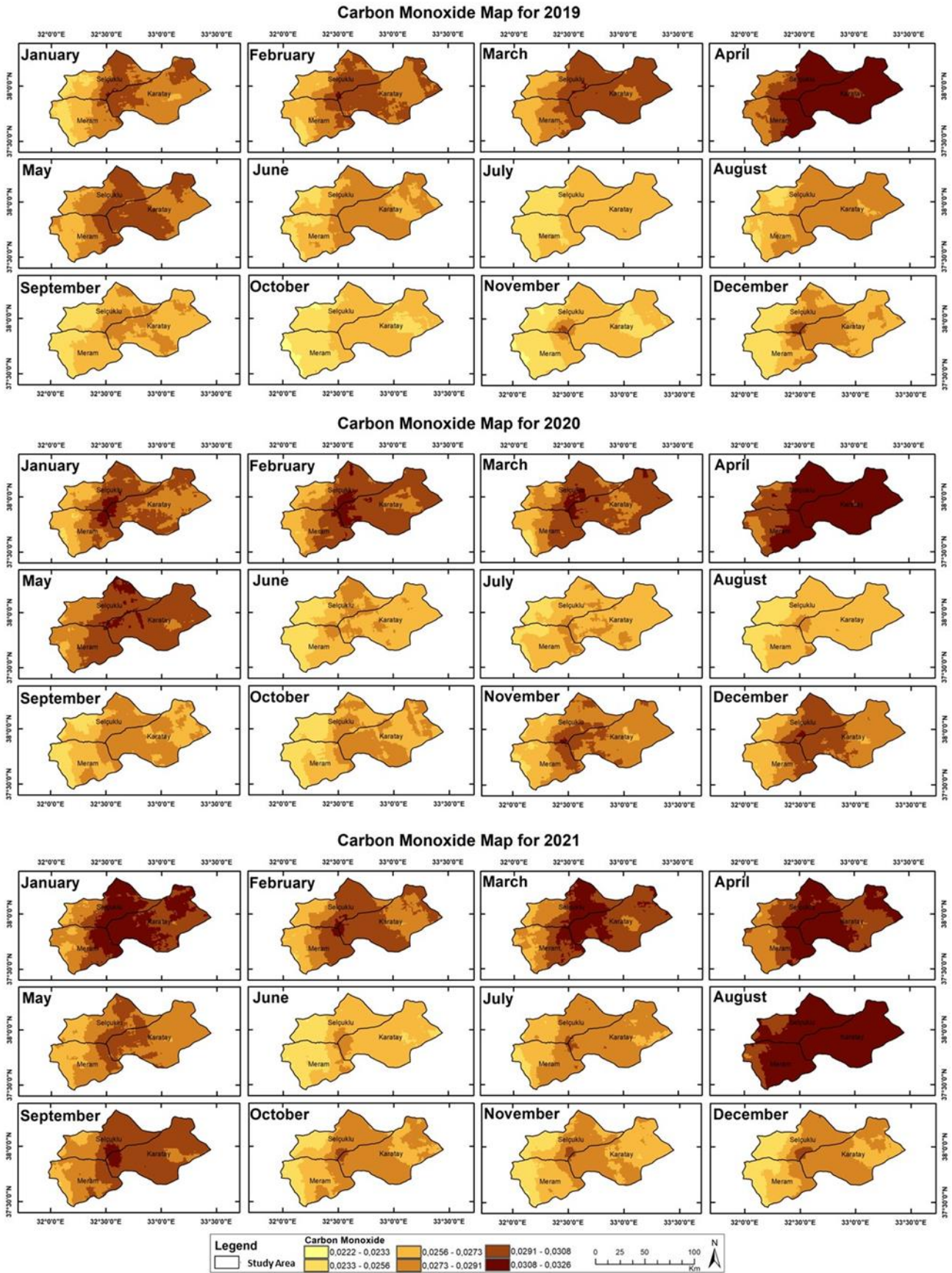
**Figure 6.** Carbon monoxide maps for 2019-2021

As a result of the combustion or incomplete combustion of the carbon in the structure of the natural gas, coal, or wood used, this gas comes out and spreads to the atmosphere. In addition, it is seen that the carbon monoxide density is higher in the city center on all maps. There is significant pollution in parts of the road network. The main reason for this is;

Gasoline is preferred in vehicles used for transportation purposes. Gasoline also has a carbon element in its chemical structure.

The carbon monoxide column densities obtained from the Sentinel-5P satellite belonging to the central districts of Konya between 2019-2021 are given in Figure 7. In the winter seasons of 2019 and 2021, it is seen that the densities are compatible with each other. As of April 2020, restrictions such as curfews have been introduced in our country to reduce the worldwide pandemic's impact. For this reason, the graph explains the decrease in carbon monoxide concentration in May compared to the previous year. In addition, the partial removal of restrictions as of June has increased the density. Again, the same factor was in question in 2021. In winter 2021, transportation was used sparingly because of the restriction's effect, which contributed to the decrease in carbon monoxide density. This density is higher in the summer of 2021 than in previous years. The main reason for this situation is that the restrictions have been reduced.
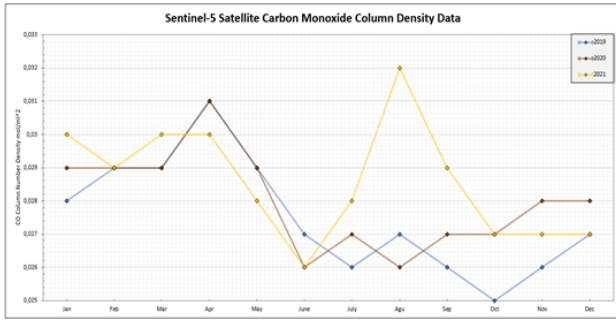


**Figure 7.** Sentinel-5 satellite carbon monoxide column number density

## 4 Conclusions

This study examined the urban heat island and carbon monoxide concentration in three central districts of Konya between 2019 and 2021. Based on the findings, the amount of heat and the increase in carbon monoxide in the city are directly proportional. This is because heat and carbon monoxide increased in the city center in 2021. This situation is also observed where transportation lines and residential areas are located. The most significant contributors to pollution in these areas are motor vehicles in traffic and home heating systems.

Additionally, when looked at seasonally, there were increases in pollutant levels in the summer of 2021 compared to the spring of 2019 and 2020. The impact of pollutants in the summer season is more significant on human health than in the winter. This is because pollutant gases from cars are found in the lower levels of the atmosphere in the summer months and disperse more slowly. In winter, pollutant gases

are dispersed to the upper levels of the atmosphere due to weather conditions (wind).

When examining the population of the study area, the most populous district is Selçuklu. The increase in air pollution in this area can be attributed, in part, to the population factor. There is no direct relationship between surface temperature and population. However, in densely populated areas, the presence of settlements, land use patterns, and urbanization can contribute to higher surface temperatures. Areas with extensive concrete structures and limited green spaces may experience the urban heat island effect, resulting in higher surface temperatures. This phenomenon can lead to hotter urban centers and relatively cooler regions in rural areas.

The amount of heat in cities also varies from region to region due to their geometric structure. An increase in heat also affects human health. Therefore, to reduce this effect in cities, reducing the concentration of carbon monoxide is necessary. Studies can be conducted to make the fuel used for heating purposes more environmentally friendly or to promote the use of environmentally friendly fuels in vehicles. Furthermore, if the NDVI index is used to determine the amount of heat, the density of green areas should be increased in areas with high heat effects or in city centers.

As a result, the size and density of the population, along with factors such as increased human activities and the resulting emissions of CO, can affect local air quality and pollutant levels. Additionally, surface temperature is closely related to urban development, land use patterns, and natural factors. Therefore, there is a proportional relationship between CO and surface temperature.

## Conflict of interest

The authors declare that there is no conflict of interest.

**Similarity rate (iThenticate):** %5

## References

[1] Ş. Durak, Geleneksel kırsal konutların ekolojik açıdan değerlendirilmesine yönelik bir model önerisi: Yalova örneği. 2021. Doktora Tezi, Kocaeli Üniversitesi Üniversitesi Fen Bilimleri Enstitüsü, Türkiye, 2021.

[2] Ü.D. Yüksel and O. Yılmaz, Ankara kentinde kentsel isi adasi etkisinin yaz aylarinda uzaktan algilama ve meteorolojik gözlemlere dayali olarak saptanmasi ve değerlendirilmesi. Gazi Üniversitesi Mühendislik Mimarlık Fakültesi Dergisi, 2008. 23(4). https://dergipark.org.tr/en/download/article-file/75772

[3] T.R. Oke, The energetic basis of the urban heat island. Quarterly Journal of the Royal Meteorological Society, 108(455), 1-24, 1982. https://www.patarnott.com/pdf/Oake1982_UHI.pdf

[4] Ö. Akyürek, Termal uzaktan algılama görüntüleri ile yüzey sıcaklıklarının belirlenmesi: Kocaeli örneği. Doğal Afetler ve Çevre Dergisi, 6(2), 377-390, 2020. https://doi.org/10.21324/dacd.667594

[5] B. Esin and N.S. Partigöç, İklim Değişikliğine Uyum Sürecinde Kent Planlamanın Rolü. Resilience, 6(1),

127-143, 2022. https://doi.org/10.32569/resilience.1026712

[6] R.C. Estoque and Y. Murayama, Monitoring surface urban heat island formation in a tropical mountain city using Landsat data (1987–2015). ISPRS Journal of Photogrammetry and Remote Sensing, 133, 18-29, 2017. https://doi.org/10.1016/j.isprsjprs.2017.09.008

[7] X. Zhang, R.C. Estoque and Y. Murayama, An urban heat island study in Nanchang City, China based on land surface temperature and social-ecological variables. Sustainable cities and society, 32, 557-568, 2017. https://doi.org/10.1016/j.scs.2017.05.005

[8] X. Zhang, R. C. Estoque, Y. Murayama and M. Ranagalage, Capturing urban heat island formation in a subtropical city of China based on Landsat images: implications for sustainable urban development. Environmental Monitoring and Assessment, 193(3), 1-13, 2021. https://doi.org/10.1007/s10661-021-08890-w

[9] Turkish Statistical Institute https://data.tuik.gov.tr/Bulten/Index?p=Dunya-Nufus-Gunu-2022-45552 , Accessed 07 December 2022.

[10] M. Poumadere, C. Mays, S. Le Mer and R. Blong, The 2003 heat wave in France: dangerous climate change here and now. Risk Analysis: an International Journal, 25(6), 1483-1494, 2005. https://doi.org/10.1111/j.1539-6924.2005.00694.x

[11] W. Zhou, G. Huang and M.L. Cadenasso, Does spatial configuration matter? Understanding the effects of land cover pattern on land surface temperature in urban landscapes. Landscape and urban planning, 102(1), 54-63, 2011. https://doi.org/10.1016/j.landurbplan.2011.03.009

[12] D. Duarte, Padrões de ocupação do solo e microclimas urbanos na região de clima tropical continental. Pós. Revista do Programa de Pós-Graduação em Arquiteturae Urbanismo da FAUUSP, 9, 88-107, 2001. https://doi.org/10.11606/issn.2317-2762.v0i9p88-107

[13] C.R.D. Almeida, L. Furst, A. Gonçalves and A. C Teodoro, Remote Sensing Image-Based Analysis of the Urban Heat Island Effect in Bragança, Portugal. Environments, 9(8), 98, 2022. https://doi.org/10.3390/environments9080098

[14] T. Mushore, J. Odindi and O. Mutanga, "Cool" Roofs as a Heat-Mitigation Measure in Urban Heat Islands: A Comparative Analysis Using Sentinel 2 and Landsat Data. Remote Sensing, 14(17), 4247, 2022. https://doi.org/10.3390/rs14174247

[15] Y.J. Choe and J.H. Yom, Improving accuracy of land surface temperature prediction model based on deep-learning. Spatial Information Research, 28(3), 377-382, 2020. https://doi.org/10.1007/s41324-019-00299-5

[16] C. Ketterer and A. Matzarakis, Comparison of different methods for the assessment of the urban heat island in Stuttgart, Germany. International journal of biometeorology, 59(9), 1299-1309, 2015. https://doi.org/10.1007/s00484-014-0940-3

[17] O. Adeyeri, A. Akinsanola and K. Ishola, Investigating surface urban heat island characteristics over Abuja, Nigeria: Relationship between land surface temperature and multiple vegetation indices. Remote Sensing Applications: Society and Environment, 7, 57-68, 2017. https://doi.org/10.1016/j.rsase.2017.06.005

[18] Ü. Güler and K. Kalkan, Sentinel-3 Verileri ile Aktif Yangın Tespiti ve Sentinel-2 Verileri ile Doğrulanması. Turkish Journal of Remote Sensing and GIS, 3(2), 86-97, 2022. https://doi.org/10.48123/rsgis.1095460

[19] Q. Zhao, L. Yu, X. Li, D. Peng, Y. Zhang and P. Gong, Progress and trends in the application of Google Earth and Google Earth Engine. Remote Sensing, 13(18), 3778, 2021. https://doi.org/10.3390/rs13183778

[20] A. Midekisa, F. Holl, D. J. Savory, R. Andrade-Pacheco, P. W. Gething, A. Bennett and H. J. Sturrock, Mapping land cover change over continental Africa using Landsat and Google Earth Engine cloud computing. PloS one, 12(9), e0184926, 2017. https://doi.org/10.1371/journal.pone.0184926

[21] B. DeVries, C. Huang, J. Armston, W. Huang, J. W. Jones and M. W. Lang, Rapid and robust monitoring of flood events using Sentinel-1 and Landsat data on the Google Earth Engine. Remote Sensing of Environment, 240, 111664, 2020. https://doi.org/10.1016/j.rse.2020.111664

[22] R. Goldblatt, W. You, G. Hanson and A.K. Khandelwal, Detecting the boundaries of urban areas in india: A dataset for pixel-based image classification in google earth engine. Remote Sensing, 8(8), 634, 2016. https://doi.org/10.3390/rs8080634

[23] J. Xiong, P. S. Thenkabail, J. C. Tilton, M. K. Gumma, P. Teluguntla, A. Oliphant and N. Gorelick, Nominal 30-m cropland extent map of continental Africa by integrating pixel-based and object-based algorithms using Sentinel-2 and Landsat-8 data on Google Earth Engine. Remote Sensing, 9(10), 1065, 2017. :https://doi.org/10.3390/rs9101065

[24] D. Arikan and F. Yildiz, Investigation of Antalya forest fire's impact on air quality by satellite images using Google earth engine. Remote Sensing Applications: Society and Environment, 100922, 2023. https://doi.org/10.1016/j.rsase.2023.100922

[25] J.A. Sobrino, R. Oltra-Carrió, G. Sòria, J. C. Jiménez-Muñoz, B. Franch, V. Hidalgo and M. Paganini, Evaluation of the surface urban heat island effect in the city of Madrid by thermal remote sensing. International journal of remote sensing, 34(9-10), 3177-3192, 2013. https://doi.org/10.1080/01431161.2012.716548

[26] S. Çobanyıldız, Konya'da şehirleşmenin sıcaklık ve yağış üzerine etkisi. Yüksek Lisans Tezi, Necmettin Erbakan Üniversitesi Fen Bilimleri Enstitüsü, Türkiye, 2016.

[27] Ş. Yaman and E.T. Görmüş, Orman Zararlılarının Verdiği Zararın Google Earth Engine Kullanılarak İzlenmesi. Turkish Journal of Remote Sensing and GIS, 3(2), 139-149, 2022. https://doi.org/10.48123/rsgis.1116907

[28] O.S. Yılmaz, M. S. Oruç, A. M. Ateş and F. Gülgen, Orman Yangın Şiddetinin Google Earth Engine ve Coğrafi Bilgi Sistemleri Kullanarak Analizi: Hatay-

Belen Örneği. Journal of the Institute of Science and Technology, 11(2), 1519-1532, 2021. https://doi.org/10.21597/jist.817900

[29] N. You and J. Dong, Examining earliest identifiable timing of crops using all available Sentinel 1/2 imagery and Google Earth Engine. ISPRS Journal of Photogrammetry and Remote Sensing, 161, 109-123, 2020. https://doi.org/10.1016/j.isprsjprs.2020.01.001

[30] N. Aslan, Landsat uydu görüntülerinden kentsel ısı adalarının belirlenmesi: Batı Akdeniz Bölgesi örneği. 2016. Yüksek Lisans Tezi, Akdeniz Üniversitesi Fen Bilimleri Enstitüsü, Türkiye, 2016.

[31] Landsat Satellite 8 Information. https://www.usgs.gov/landsat-missions/landsat-8?qt-science_support_page_related_con=0#qt-science_support_page_related_con , Accessed 07 December 2022.

[32] R. Yunita, A. Wibowo and A. Rais. Urban Heat Island Mitigation Strategy based on Local Climate Zone Classification using Landsat 8 satellite imagery. in IOP Conference Series: Earth and Environmental Science. 2022. IOP Publishing. https://doi.org/10.1088/1755-1315/1039/1/012013

[33] S.S. Arifin, B. Hamzah, R. Mulyadi and A. R. Rasyid, Effects of Vegetation on Urban Heat Island Using Landsat 8 OLI/TIRS Imagery in Tropical Urban Climate, 10, 395-405, 2022. https://doi.org/10.13189/cea.2022.100134

[34] C. Xu, G. Chen, Q. Huang, M. Su, Q. Rong, W. Yue and D. Haase, Can improving the spatial equity of urban green space mitigate the effect of urban heat islands? An empirical study. Science of The Total Environment, 841, 156687, 2022. https://doi.org/10.1016/j.scitotenv.2022.156687

[35] X. Yu, X. Guo and Z. Wu, Land surface temperature retrieval from Landsat 8 TIRS—Comparison between radiative transfer equation-based method, split window algorithm and single channel method. Remote sensing, 6(10), 9829-9852, 2014. https://doi.org/10.1016/j.isprsjprs.2020.01.001

[36] M. Jin, J. Li, C. Wang and R. Shang, A practical split-window algorithm for retrieving land surface temperature from Landsat-8 data and a case study of an urban area in China. Remote sensing, 7(4), 4371-4390, 2015. https://doi.org/10.3390/rs70404371

[37] A. Sekertekin, S.H. Kutoglu and S. Kaya, Evaluation of spatio-temporal variability in Land Surface Temperature: A case study of Zonguldak, Turkey. Environmental monitoring and assessment, 188(1), 1-15, 2016. https://doi.org/10.1007/s10661-015-5032-2

[38] F. Wang, Z. Qin, C. Song, L. Tu, A. Karnieli and S. Zhao, An improved mono-window algorithm for land surface temperature retrieval from Landsat 8 thermal infrared sensor data. Remote sensing, 7(4), 4268-4289, 2015. https://doi.org/10.3390/rs70404268

[39] D. Arıkan and F. Yıldız, Türkiye'de COVID-19 döneminde NO2 emisyonunun analizi. Türkiye Ulusal Fotogrametri ve Uzaktan Algılama Birliği, sayfa 6-9, Mersin, Türkiye, 12-14 Mayıs 2022.

[40] N. Polat, Mardin ilinde uzun yıllar yer yüzey sıcaklığı değişiminin incelenmesi. Türkiye Uzaktan Algılama Dergisi, 2(1), 10-15, 2020. https://dergipark.org.tr/en/pub/tuzal/issue/52699/649526

[41] J. Zhang, Y. Wang and Y. Li, A C++ program for retrieving land surface temperature from the data of Landsat TM/ETM+ band6. Computers & geosciences, 32(10), 1796-1805, 2006. https://doi.org/10.1016/j.cageo.2006.05.001

[42] J.W. Rouse Jr, R. H. Haas, D. W. Deering, J. A. Schell and J. C. Harlan, Monitoring the vernal advancement and retrogradation (green wave effect) of natural vegetation. 1974. https://ntrs.nasa.gov/api/citations/19750020419/downloads/19750020419.pdf

[43] N. Çağlayan, Seralar için led lambalı aydınlatma otomasyon sisteminin tasarlanmasına ve uygulanmasına yönelik bir çalışma. 2013.

[44] K.J. McCree, Test of current definitions of photosynthetically active radiation against leaf photosynthesis data. Agricultural meteorology, 10, 443-453, 1972. https://doi.org/10.1016/0002-1571(72)90045-3

[45] National Air Quality Monitoring Network. http://sim.csb.gov.tr/ , Accessed 09 December 2022.